Bioconjugate Chemistry

Article

pubs.acs.org/bc

Synthesis and Biodistribution Studies of ^{3}H- and ^{64}Cu-Labeled Dendritic Polyglycerol and Dendritic Polyglycerol Sulfate

Kritee Pant,[†] Dominic Gröger,[‡] Ralf Bergmann,[†] Jens Pietzsch,[†,§] Jörg Steinbach,[†,§] Bim Graham,[∥] Leone Spiccia,[⊥] Fannely Berthon,[#] Bertrand Czarny,[#] Laurent Devel,[#] Vincent Dive,*[,#] Holger Stephan,*[,†] and Rainer Haag*[,‡]

[†]Helmholtz-Zentrum Dresden - Rossendorf, Institute of Radiopharmaceutical Cancer Research, Bautzner Landstrasse 400, D-01328 Dresden, Germany

[‡]Organische Chemie, Institut für Chemie und Biochemie, Freie Universität Berlin, Takustrasse 3, D-14195, Berlin, Germany

[§]Technische Universität Dresden, Department of Chemistry and Food Chemistry, D-01062 Dresden, Germany

[∥]Monash Institute of Pharmaceutical Sciences, Monash University, Parkville, VIC 3052, Australia

[⊥]School of Chemistry, Monash University, Clayton, VIC 3800, Australia

[#]CEA-Saclay, Service d'Ingénierie Moléculaire de Protéines (SIMOPRO), Labex LERMIT, CEA-DSV-iBiTecS, 91191 Gif/Yvette Cedex, France

Supporting Information

ABSTRACT: Dendritic polyglycerol sulfate (dPGS) is a biocompatible, bioactive polymer which exhibits anti-inflammatory activity in vivo and thus represents a promising candidate for therapeutic and diagnostic applications. To investigate the in vivo pharmacokinetics in detail, dPGS with a molecular weight of approx. 10 kDa was radiolabeled with ^{3}H and ^{64}Cu, and evaluated by performing biodistribution studies and small animal positron emission tomography (PET). ^{3}H-labeling was accomplished by an oxidation−reduction process with sodium periodate and [^{3}H]-borohydride. ^{64}Cu-labeling was achieved by conjugation of isothiocyanate- or maleimide-functionalized copper(II)-chelating ligands based on 1,4-bis(2-pyridinylmethyl)-1,4,7-triazacyclononane (DMPTACN) to an amino functionalized dPGS scaffold, followed by reaction with an aqueous solution containing $^{64}CuCl_2$. Independent biodistribution by radioimaging and PET imaging studies with healthy mice and rats showed that the neutral dPG was quantitatively renally eliminated, whereas the polysulfated analogues accumulated mainly in the liver and spleen. Small amounts of the dPGS derivatives were slowly excreted via the kidneys. The degree of uptake by the reticuloendothelial system (RES) was similar for dPGS with 40% or 85% sulfation, and surface modification of the scaffold with the DMPTACN chelator did not appear to significantly affect the biodistribution profile. On the basis of our data, the applicability of bioactive dPGS as a therapeutic agent might be limited due to organ accumulation even after 3 weeks. The inert characteristics and clearance of the neutral polymer, however, emphasizes the potential of dPG as a multifunctional scaffold for various nanomedical applications.

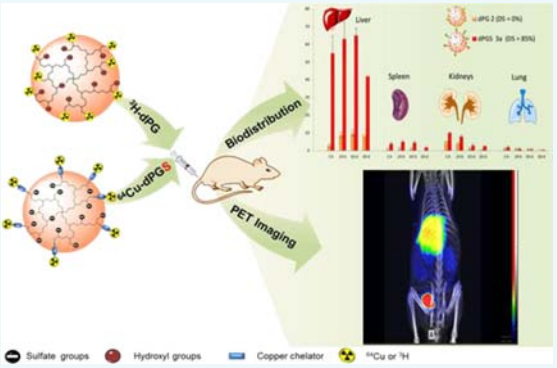

INTRODUCTION

Dendritic polyglycerols (dPGs) are nanoscaled, water-soluble polyether polyols that exhibit excellent biocompatibility and can be synthesized in a single step with predetermined molecular weight and narrow polydispersity.[1,2] Their derivatives have been explored in a variety of biological applications, such as protein resistant surface coatings, bioactive agents, and delivery systems.[3−5] In 2004, a polysulfated analogue of dPG was developed, so-called "dendritic polyglycerol sulfate" (dPGS), which exhibits lower anticoagulative and enhanced anti-inflammatory activity when compared to heparin.[6] dPGS and its derivatives were found to block the binding of L- and P-selectins to their natural ligands—an essential step in the inflammatory processes—and also to efficiently inhibit the complement system.[4] Based on these strong multivalent interactions, dPGS−dye conjugates were successfully applied as imaging agents in inflammatory disease models, such as for rheumatoid arthritis and acute asthma.[7,8] For preclinical development, however, it is necessary to obtain reliable biodistribution profiles that allow the in vivo fate of these nano-objects to be determined. For applications requiring long plasma half-life, e.g., in drug delivery, uncharged high-molecular

Received: March 5, 2015
Revised: April 17, 2015
Published: April 19, 2015

DOI: 10.1021/acs.bioconjchem.5b00127
Bioconjugate Chem. 2015, 26, 906−918

Scheme 1. Synthesis of ^{3}H-Labeled Dendritic Polyglycerol Derivatives (^{3}H-dPG, ^{3}H-dPGS), Bifunctional DMPTACN-Based Chelators, and ^{64}Cu-Labeled Dendritic Polyglycerol Sulfates (^{64}Cu-dPGS-DMPTACN conjugates)[a]

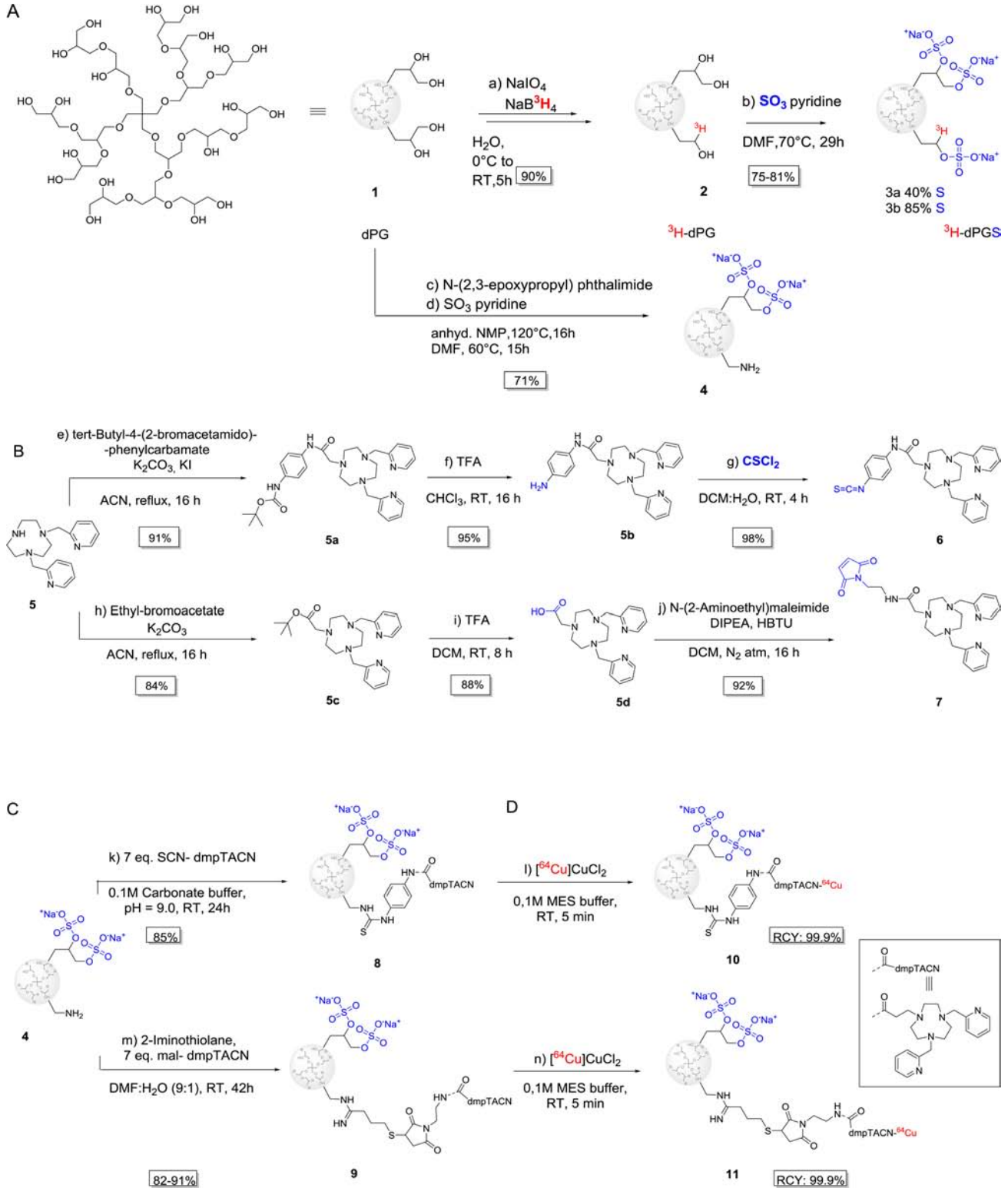

[a](A) Idealized chemical structure of dPG **1** and synthesis of ^{3}H-labeled dPG (**2**, ^{3}H-dPG) and subsequent sulfation with SO_3 pyridine complex to give **3a** (DS = 40%) and **3b** (DS = 85%). (B) Synthesis of bifunctional isothiocyanate- (**6**) and maleimide- (**7**) functionalized DMPTACN ligands for Cu(II) chelation. (C) Conjugation of DMPTACN ligands to dPGS amine **4** via direct coupling of **6** to yield **8**, or via thiolation with 2-iminothiolane and subsequent Michael addition with **7** to yield **9**. (D) ^{64}Cu(II) complexation by the dPGS-DMPTACN conjugates **8** and **9** to yield **10** and **11**, respectively.

DOI: 10.1021/acs.bioconjchem.5b00127
Bioconjugate Chem. 2015, 26, 906−918

weight polyglycerols (>100 kDa) and their derivatives are best suited, whereas for "low" molecular weight dPG and its derivatives (<50 kDa), rapid elimination from the systemic circulation is desired.[9,10] The most important factors to be considered in this respect are the polymer size, charge, hydrophobicity, and surface properties.[11,12] It is generally accepted that neutral, soft "stealth" polymer scaffolds with a molecular weight below 40 kDa are predominantly eliminated via renal filtration. In contrast, charged or hydrophobic macromolecules of comparable molecular weight usually associate with or bind to biological entities such as plasma proteins or cell surfaces. As a result, they are rapidly eliminated via and deposited in organs of the reticuloendothelial system (RES).[13−15]

To better understand the metabolic fate of dPGs, radiolabeling is the method of choice because it allows for sensitive, reliable ex vivo and in vivo imaging with high temporal resolution. So far, labeling of dPGS has been achieved only by radiosulfation of dPG N-phthalimide derivatives with the $^{35}SO_3$-pyridine complex, and autoradiography used to obtain ex vivo data about the tissue and cellular localization of ^{35}S-labeled dPGS.[16,17] A drawback of this approach is the potential for hydrolytic cleavage of the sulfoester bond in vivo, which cannot be excluded as a possibility. Moreover, the behavior of the neutral polymer cannot be investigated using this labeling approach.

With the above in mind, we sought to develop synthetic strategies to access ^{3}H-labeled and ^{64}Cu-labeled dPGs, the details of which are reported herein. Radiolabeling of dendritic polyglycerols with ^{3}H ($t_{1/2}$ = 12.3 y) provides a cheaper and more straightforward alternate to ^{35}S-labeling, and also allows the ex vivo biodistribution to be studied over a longer time frame. Furthermore, with the development of digital radioimagers, quantitative and high resolution distribution of labeled compounds in tissue sections can be performed.[47] ^{64}Cu-labeled dPGs can be employed in positron emission tomography (PET), which has emerged as an important diagnostic tool for the visualization of biological and pathophysiological processes, and permits quantification of biodistribution and pharmacokinetic data in vivo.[18] Due to the favorable decay characteristics of ^{64}Cu ($t_{1/2}$ = 12.7 h, β^+ = 19%; β = 40%; electron capture 40%), this radioisotope has received significant attention in the PET field.[19−22] Since dPGs do not have any metal binding sites, it was important to couple chelators capable of forming stable ^{64}Cu(II) complexes to the dPG scaffolds. A wide range of copper(II)-binding chelating ligands are already known and promising platforms based on bispidine and 1,4,7-triazacyclononane (TACN) have been developed by our group over the years.[23−29]

As part of this work, we report the synthesis of two new derivatives of 1,4-bis(2-pyridinylmethyl)-TACN (DMPTACN) featuring maleimide and isothiocyanate coupling groups to enable conjugation to polyglycerol derivatives bearing mercapto or amino groups. Efficient approaches for labeling dendritic polyglycerol derivatives with ^{3}H and ^{64}Cu radionuclides are also described, together with a new radiometric titration assay for the characterization of ^{64}Cu-labeled dPGs. The latter provides an efficient and sensitive procedure for detecting even slight modifications of the polymer (nmol), with much smaller amounts of sample required in comparison to NMR spectroscopic analysis. Using these easily accessible ^{3}H- and ^{64}Cu-radiolabeled compounds, reliable information about the biodistribution of dPG could be obtained using a combination of liquid scintillation counting, radioimaging (^{3}H), and small animal PET (^{64}Cu). This paper compares, for the first time, the biodistribution of dPG and dPGS derivatives, which will help pave the way toward inflammation-specific multimodal imaging agents.

RESULTS AND DISCUSSION

Synthesis of ^{3}H-Labeled dPG and dPGS. Dendritic polyglycerol (dPG **1**, Scheme 1) was prepared via an anionic ring-opening multibranching polymerization (ROMBP) reaction of glycidol with a deprotonated pentaerythritol starter.[1,30] The polymer has an average molecular weight (M_n) of 6000 g mol^{-1}, a degree of branching (DB) of 60%, a polydispersity index (PDI, M_w/M_n) of <1.6, and a hydrodynamic diameter of 5 ± 1.5 nm (as determined by dynamic light scattering, DLS).[34] Tritium-labeled dPG (^{3}H-dPG **2**, Scheme 1A) was synthesized by partial oxidative cleavage of terminal 1,2-diol units and subsequent reduction of the intermediate aldehydes with [^{3}H]-sodium borohydride. This method has so far only been applied to 1,2-diol-containing small molecules like carbohydrates[31] and represents a mild, straightforward labeling technique for the introduction of deuterium or tritium into 1,2-diol-containing molecules or polymers without the need for radioactive monomers. In this particular case, the chemical structure of the polyglycerol scaffold is hardly altered because only a few terminal diols are converted to terminal ethylene glycol units, which are known to be highly biocompatible and are closely related in structure to the dPG subunits. By optimizing the reaction parameters, a radiochemical yield of >80% was reached, highlighting the efficiency of this reaction. Furthermore, this method provides an alternative for the ^{3}H-methylation of polyglycerols using base and tritiated methyl iodide, as frequently applied by Brooks and co-workers.[9,32,33] Polysulfated ^{3}H-dPGS derivatives **3a** and **3b** were prepared by reacting **2** with sulfur trioxide pyridine complex at 70 °C in DMF to directly convert the hydroxyl groups into sulfate groups.[34] In order to evaluate the impact of the degree of sulfation (DS) on biodistribution, two polymers were prepared, one with a DS of 40% (**3a**) and another with a DS of 85% (**3b**). The final polysulfates **3a** and **3b** had average molecular weights of 9300 and 13 000 g mol^{-1}, and hydrodynamic diameters of 6 ± 1.5 nm, respectively. In contrast to the recently reported ^{35}S radiosulfation method, the approach described herein avoids the possibility of hydrolytic cleavage of the sulfoester group and also allows the biodistribution of the neutral precursor polymer to be investigated.[16] In all cases, any free tritium was removed by ultrafiltration and size exclusion chromatography (SEC).

Synthesis of Conjugatable TACN-Based Chelators. TACN-based ligands are known to form highly stable copper(II) complexes.[22,26] The incorporation of two pyridine-containing pendants to produce DMPTACN further enhances the affinity for Cu(II) ($\log K_{Cu\text{-}L}$ > 25). The remaining secondary amine of DMPTACN can be functionalized to facilitate attachment to other molecules, e.g., biomolecules.[28,29] In this work, the synthesis of two new DMPTACN-based bifunctional chelators (BFCs) for introduction of the positron-emitting radionuclide ^{64}Cu was achieved according to Scheme 1B. The first BFC, SCN-DMPTACN **6**, features an isothiocyanate group to allow direct coupling to the amino groups of dPGS amine **4**. It was prepared via reaction of the previously reported compound amino-DMPTACN (**5b**)[35] with thiophosgene. The reaction was carried out in the presence of

DOI: 10.1021/acs.bioconjchem.5b00127
Bioconjugate Chem. 2015, 26, 906−918

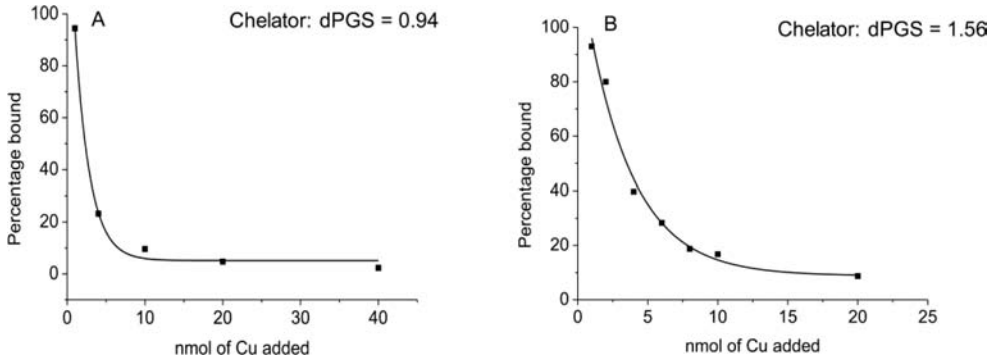

Figure 1. Percentage of Cu(II) specifically bound to dPGS-DMPTACN conjugate **8** (A) and dPGS-DMPTACN conjugate **9** (B) versus moles of Cu(II) added ([dPGS-DMPTACN conjugate] = 0.2 mM), as determined by radio-TLC analysis.

water, resulting in in situ dehydrohalogenation of the initially formed thiocarbamoyl chloride intermediate. The product was purified via high pressure liquid chromatography (HPLC) and characterized using thin-layer chromatography (TLC), ESI-MS, and NMR spectroscopy (Figure S1). The second BFC, mal-DMPTACN **7**, incorporates a maleimide group introduced via a nucleophilic acyl substitution reaction between the carboxylic group of DMPTACN acetic acid[26] and *N*-(2-aminoethyl) maleimide, with HBTU used as an activating agent. The reaction was performed in DMF and the crude product was used without purification to avoid hydrolysis of the maleimide group. ESI-MS confirmed the formation of **7** and any side-products were found not to interfere with subsequent conjugation to mercapto (-SH) groups introduced onto a dPGS scaffold (vide infra).

Conjugation of TACN-Based Chelators to dPGS. Partially aminated dPGS (dPGS amine **4**) was prepared by a recently reported sequential copolymerization approach involving the use of N-phthalimide functionalized monomer units. The phthalimide protecting groups were then removed to expose reactive amino groups for conjugation.[16] The dPGS amine **4** had a DS of 85%, and $M_n \approx 10\,000$ g mol^{-1}, a DB of 60%, a PDI of <1.6, and a hydrodynamic diameter of 5.6 ± 1.2 nm, comparable to that of ^{3}H-dPGS **3b**. Direct coupling of SCN-DMPTACN to the amine groups of dPGS amine **4** was performed in 100 mM carbonate buffer (pH 9) at room temperature for 24 h (Scheme 1C). By using equimolar amounts of reactants, a labeling yield of 0.96 chelator units per polymer **8** was achieved, as determined by radiometric titration (Figure 1A). The second BFC, mal-DMPTACN **7**, was conjugated to dPGS amine **4** after thiolation of the polymer with 2-iminothiolane in the presence of DIPEA in a DMF/water mixture. Conjugation was then achieved by a Michael addition reaction between the maleimide group of mal-DMPTACN **7** and the thiolated dPGS, carried out at room temperature for 42 h (Scheme 1C). A labeling yield of 1.56 chelator units per polymer **9** was achieved, as determined by ^{1}H NMR spectroscopy (Figure S2) and radiometric titration (Figure 1B). The conjugates were purified via SEC using Sephadex G-25, and obtained in yields of 85% (**8**) and 82−91% (**9**), respectively. The purity was confirmed by analytical SEC (Figure S3). Modification of the dPGS scaffolds with the BFCs did not affect the hydrodynamic size.

^{64}Cu-Labeling and In Vitro Stability of ^{64}Cu-dPGS-DMPTACN Conjugates. The dPGS-DMPTACN conjugates **8** and **9** were labeled with ^{64}Cu in 2-[*N*-morpholino]-ethansulfonic acid (MES)/NaOH buffer. Aliquots of a stock solution of ^{64}Cu[Cu]Cl$_2$ were added to solution of **8** and **9** dissolved in 100 mM of MES buffer (pH 5.5), and the extent of labeling was measured after different periods of incubation at room temperature (up to 24 h). To assess the rate of complexation, radio-TLC was conducted at different time intervals (Figure S4). The radiolabeled dPGS-DMPTACN derivatives **10** and **11** remain at the origin and ^{64}CuCl$_2$ moves with the solvent front. These studies showed labeling yields of >99% within 5 min. Radio-SEC experiments confirmed a high radiochemical purity, obviating the need for further steps to remove any contaminants (Figure S5). Effective specific activities of 15 GBq μmol^{-1} (405 mCi μmol^{-1}) and 13 GBq μmol^{-1} (351 mCi μmol^{-1}) for **10** and **11**, respectively, have been obtained.

Stable ^{64}Cu(II) complex formation and high resistance of **10** and **11** to metal ion leaching was confirmed through challenge experiments performed with up to a 100-fold excess of cyclam and in the presence of 0.1 M EDTA (Figures S6 and S7). There was no evidence of transchelation for the ^{64}Cu-labeled dPGS-DMPTACN conjugates, even after 24 h of incubation. The dPGS amine **4** showed negligible amounts of ^{64}Cu binding.

Radiochemical Determination of the Chelator-to-Polymer Ratio. In order to further characterize the DMPTACN-dPGS conjugates, a radiometric titration assay was developed which could be used to determine the number of chelate units per dPGS molecule, and employed only nanomolar amounts of sample. Radionuclides, such as ^{57}Co, have been used in the past to determine the number of ligands attached to antibodies.[36,37] The major advantage of this procedure is the low amount of sample (μg) required for detection. The radiometric titration method exploits the fact that the dPGS amine scaffold itself does not bind Cu(II) ions. To confirm this, an excess of EDTA was added after complex formation. Subsequent radio-TLC analysis showed that the amount of nonspecifically bound Cu(II) was negligible. Therefore, the amount of Cu(II) bound to the dPGS-DMPTACN conjugates **8** and **9** corresponds to the number of bound chelators/chelates. In the titration, increasing amounts of a mixture of radioactive and nonradioactive Cu(II) were added to a fixed amount of conjugate sample and the complexation monitored via radio-TLC. By plotting the percentage of Cu(II) bound against the total concentration of the Cu(II) added, the ratio (nmol) of chelator/chelate present per nmol of the polymer could be determined (Figure 1A and B). The results from this analysis were in agreement with NMR data (Figure S2). Radiometric titration may represent a reliable

DOI: 10.1021/acs.bioconjchem.5b00127
Bioconjugate Chem. 2015, 26, 906−918

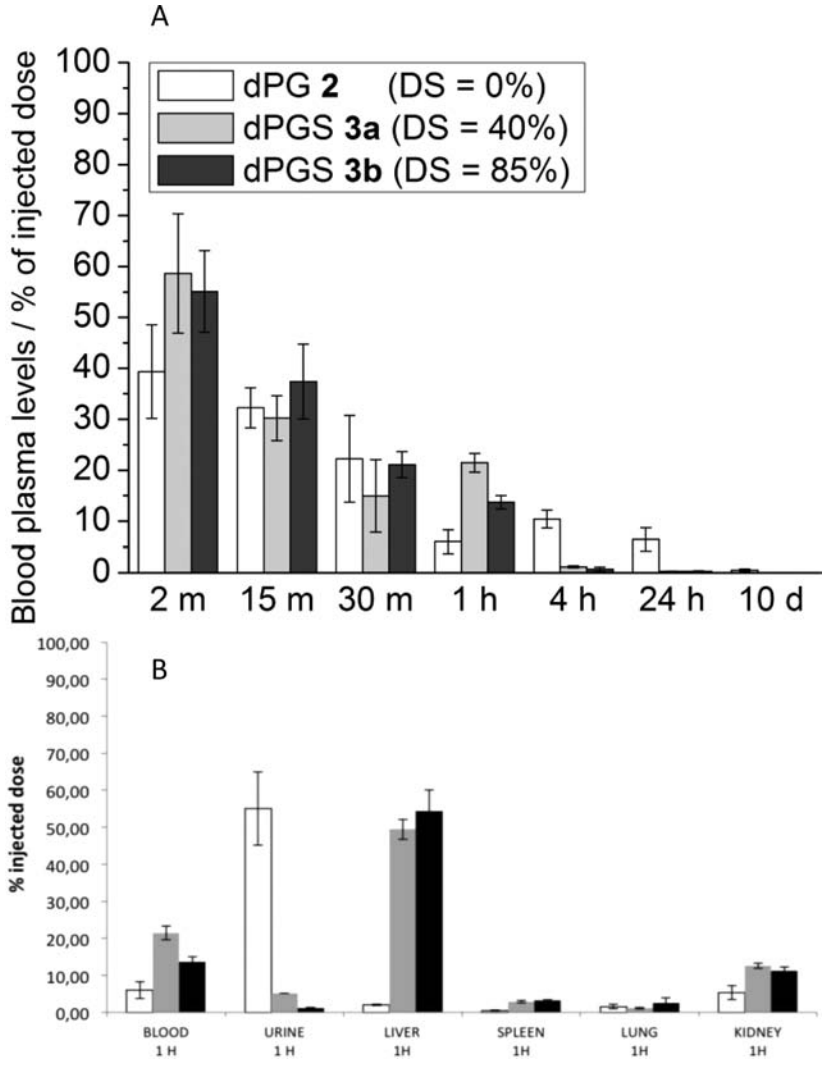

Figure 2. (A) Content of tritiated dPG **2** and dPGS **3a** (DS = 40%) and **3b** (DS = 85%) in blood plasma as a percentage of the injected dose at different time points. (B) Fluids and tissue biodistribution of polymers **2**, **3a**, and **3b** 1 h after injection.

method for characterization of other conjugates, nanoparticles, and so forth that are only available in small quantities.

Biodistribution Studies of ^{3}H-dPG and ^{3}H-dPGS. Biodistribution studies with the tritiated polymers **2**, **3a** (DS = 40%), and **3b** (DS = 85%) were conducted at the CEA in Saclay, France in compliance with National Animal Welfare Regulations. Healthy, female BALB/c mice were injected intravenously (bolus) into the tail vein with the polymers and held in metabolic cages. During the study, no signs of toxicity or adverse effects were observed and the mice grew normally. At different time points, the mice were terminated by NaCl perfusion (3 mice per time point) in order to exclude radioactivity from blood when quantifying the activity of the individual organs. The amount of polymer in blood and urine was quantified by liquid scintillation counting and their biodistribution study was performed by radioimaging of representative organ tissue sections (thickness 20 μm) following a protocol reported elsewhere.[47] The levels of polymer circulating in the blood are shown at given time points in Figure 2a. More than 50% of the neutral, hydroxyl-terminated polymer **2** ($M_n \approx 6000$ g mol^{-1}) was eliminated from the circulation after 2 min. The polysulfates (**3a**, $M_n \approx 9300$ g mol^{-1} and **3b**, $M_n \approx 13\,000$ g mol^{-1}) were initially present in larger amounts, but showed a faster clearance and were quantitatively removed from circulation in less than 4 h, while approximately 10% of neutral dPG **2** was still present in the plasma after 4 h. The above data suggest that these polymers have a two-phase blood clearance with an initial-phase half-clearance time from 2 min (neutral polymer) up to 10−15 min (polysulfate polymers) and a longer second-phase half-clearance time (from 1 to 4 h). A statistically significant, though minor effect of the degree of sulfation on the concentration of the dPGS present in plasma was only apparent after 1 h, at which time approximately 22% of the injected dPGS **3a** (DS = 40%) was found compared to 14% of **3b** (DS = 85%) (Figure 2b). The extent to which this may have been caused due to redistribution processes between different compartments could not be determined on the basis of our data.

When investigating the organ distribution, the kidneys were the target organ for the neutral polymer, with approximatively 8% of the injected dose observed in these organs, 1 h after the polymer injection. Renal clearance of **2** was confirmed by the high level of **2** (~50%) detected in urine at 1 h. In contrast, polymers **3a** and **3b** were cleared by a different pathway, as exemplified by the low level of radioactivity in urine and the high level in liver, 1 h after injection (Figure 2b). At all time

DOI: 10.1021/acs.bioconjchem.5b00127
Bioconjugate Chem. 2015, 26, 906−918

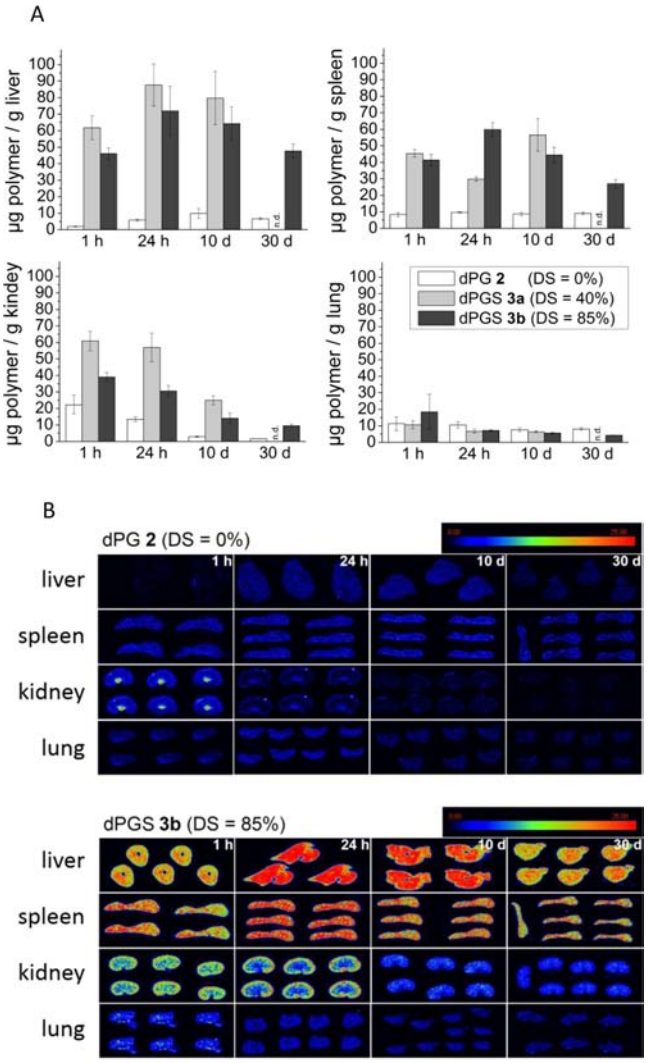

Figure 3. Distribution of ^{3}H-dPG **2**, ^{3}H-dPGS **3a** (DS = 40%), and ^{3}H-dPGS **3b** (DS = 85%) in selected organs at different time points. (A) Accumulation in liver, spleen, kidney, and lung (in μg polymer per g tissue), determined by radioimaging counting. (B) After polymer injection, three to six pieces of tissue sections were placed on a glass support and analyzed by radioimaging. Radioimaging analysis confirms the marked difference in tissue distribution between **2** and **3b**.

points, dPGSs **3a** and **3b** exhibited a larger tissue distribution than dPG **2** in all organs, even in kidneys (Figure 3). With the exception of kidneys, once in tissues all three polymers exhibited a very slow organ clearance, with 10% and 40% of the injected dose still observed in liver for dPG **2** and dPGSs **3a**, respectively, 30 d after polymer injection (Figure 4). In kidneys, slow excretion of polymers **3a** and **3b** is probably related to their accumulation in cortex as illustrated by radioimaging (see image at 24 h), showing similar behavior to that of negatively charged proteins. These results are in accordance with previous studies with ^{35}S-labeled dPGS derivatives containing free amine groups[16,17] as well as a dPGS indocarbocyanine (ICC) conjugate.[7]

For the other organs, such as the heart, thymus, and pancreas, the sum of the activity was found to be less than <1% of the injected dose for both the neutral polymer **2** and the polysulfates **3a** and **3b** at all time points (Figure S8). The former polymer accumulated only in very small amounts in the

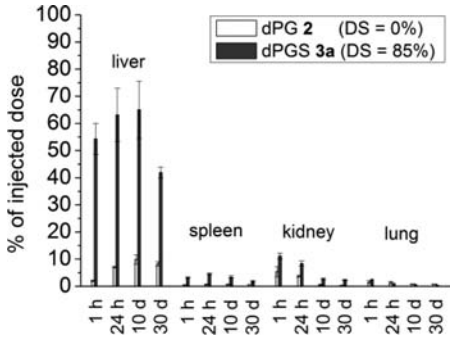

Figure 4. Organ distribution of ^{3}H-dPG **2** and ^{3}H-dPGS **3b** (DS = 85%) in selected organs at different time points as a percentage of the injected dose. Hydroxyl-terminated ^{3}H-dPG **2** is fully eliminated via kidney filtration, with a weak accumulation observed in liver (less than 10% of the injected dose after 30 d) In spleen and lung, levels of ^{3}H-dPG **2** remains lower than 1% of the injected dose. ^{3}H-dPGS **3b** accumulates to more than 60% of the injected dose in the liver after 10 d. At the end of the study (30 d), 40% of the injected dose was still found in the liver, whereas the amount in the kidneys and all other tested organs was less than 20% altogether.

bone marrow, while a sustained signal was observed for **3a** and **3b** (Figure S9). These observations are in line with the presence of **3a** and **3b** in liver and spleen, suggesting that opsonization of **3a** and **3b** directs these polymers toward resident macrophages of these organs and their phagocytosis. In the case of bone marrow, the incorporation of the polyanion **3a** and **3b** into the inorganic compartments could also be due to the capture of the polyanions by the macrophages in the bone marrow (Figure S9). A similar behavior was observed in the recent in vitro studies where it was hypothesized that the dPGS shows some affinity for hydroxyl apatite.[38] The detailed behavior is still under investigation. Uptake into the brain could not be observed; only a faint radioactivity signal was detected in ventricles for dPGS **3a** and **3b** (Figure S10). These findings suggest that, under healthy conditions, neither neutral dPG **2** nor dPGS **3a** and **3b** crosses the blood brain barrier (aggregates of dPGS and plasma proteins may, however, lead to a completely different behavior, which is currently under investigation).

In conclusion, most of the neutral polymer was cleared through the kidneys, whereas the polysulfate was deposited in large amounts in the organs of the RES (liver, spleen, and bone marrow). After several days, low activity of **3b** was measured in the feces, while the polymer concentration in the liver and spleen slowly decreased. This suggests a slow hepatobiliary excretion pathway for the sulfated polymers after hepatocyte phagocytosis or a slow metabolism of these polymers in Kuppfer cells. Even though degradation of the polyether backbone of dPG and dPGS, as well as sulfoester hydrolysis, is unlikely, this possibility cannot be totally ruled out.

In Vivo PET Studies of ^{64}Cu-dPGS in Wistar Rats. Dynamic PET imaging studies of the ^{64}Cu-labeled dPGS polymers **10** and **11** (DS = 85%) were conducted in healthy Wistar rats after single intravenous injection in the tail vein with an activity of ~100 MBq per 200 μg sample at 5 min. The PET kinetics of **10** and **11** showed similar in vivo patterns. A maximum intensity projection (MIP) of a whole body PET image of the ^{64}Cu-labeled conjugate **10** can be seen in Figure 5. Within 2 min post injection (p.i.), a strong accumulation was seen mainly in the liver, as well as the spleen (Figure 6B), with a small amount of accumulation in the kidney cortex at the

DOI: 10.1021/acs.bioconjchem.5b00127
Bioconjugate Chem. 2015, 26, 906−918

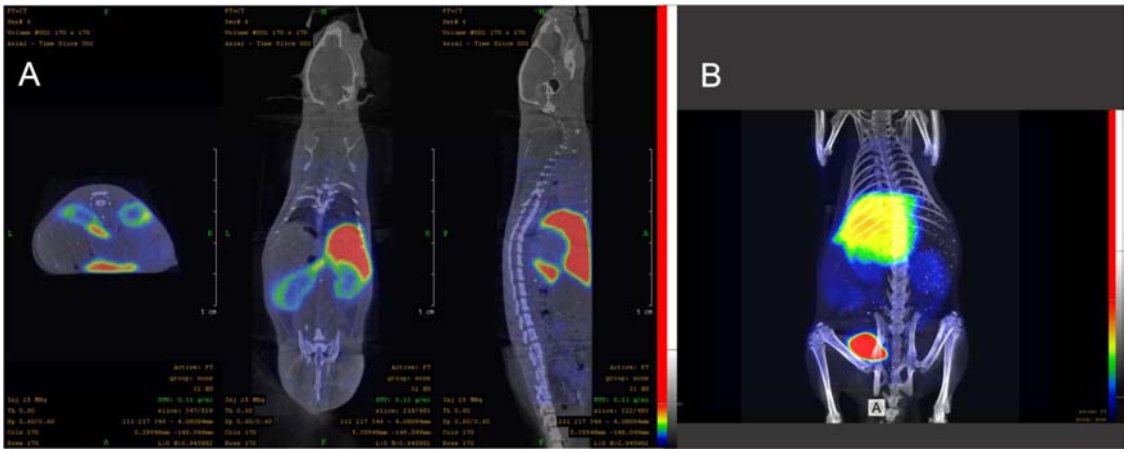

Figure 5. Whole body in vivo biodistribution of **10** in a healthy Wistar rat 90 min p.i. using positron emission tomography (PET/CT image): (A) orthogonal (transaxial, coronal, sagittal) sections, (B) maximum intensity projection (MIP).

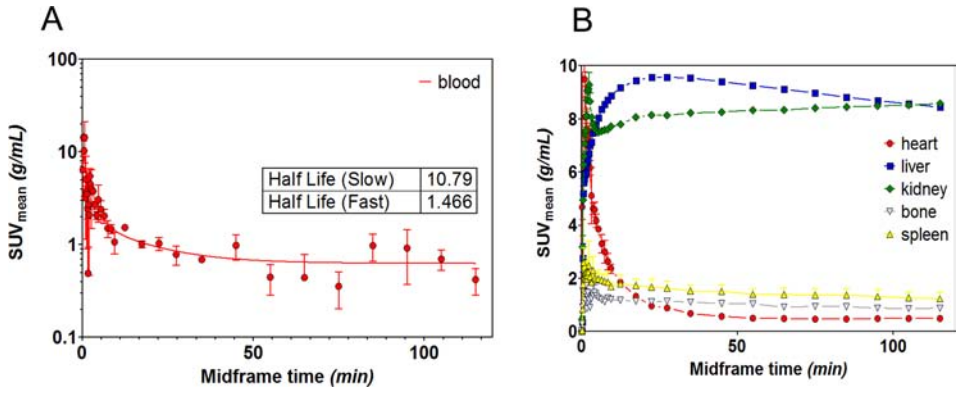

Figure 6. Graphical representation of the whole body in vivo biodistribution of **10** in a healthy Wistar rat 90 min p.i. using positron emission tomography: (A) blood half-life, (B) different organ distribution after single intravenous injection in Wistar rats. Data are given in mean ± SEM (standard error of the mean) in standard uptake value (SUV, in units of grams per milliliter), defined as the tracer concentration at a certain time point normalized to injected dose per unit body weight.

early time points. The main excretion route of the polymers was hepatobiliary and small amounts were renally excreted. The blood plasma half-life was between 1 and 11 min (Figure 6A). Slight accumulation observed in the bone marrow could be explained by entrapment of the polyanionic polymers in the macrophages of the bone marrow. Strong uptake by the RES is already known for such charged particles, which, in contact with the plasma, might interact with various proteins and form a so-called "protein corona".[46] Since the neutral ^{3}H-labeled polymer **2** showed no uptake by the RES, this effect suggests a dependence on charge.

Charged "blocking agents", e.g., lysine, have previously been employed to minimize the kidney uptake of small molecules such as radiolabeled peptides via electrostatic interactions.[45,48] In a similar way, "cold" counterparts of the radiolabeled compounds can be employed to block uptake as well as to determine any saturable processes in the organs. In order to determine if the overall biodistribution in organs is dependent on the total injected mass, the nonradioactive polymers **8** and **9** (50-fold excess) were simultaneously injected with the radiolabeled analogues (to increase the total injected mass without altering activity). These blocking/saturation studies showed a significant decrease in the liver uptake (Figure 7). This behavior could be related to the saturation of the uptake processes and/or the binding sites (possibly scavenger receptors) especially in the liver. Figure 8 shows a slightly higher kidney uptake in a maximum intensity PET image of compound **11** without (control) and with (blocked) the co-injection of the nonradiolabeled counterpart. The higher kidney uptake could be explained since the simultaneous injection of an excess of nonradiolabeled polymers reduces the unspecific binding in all the organs. Therefore, a larger amount (compared to without blocking) is detected in the blood and thus, subsequently, in the kidney. However, it is important to mention here that no significant blocking effect was seen in the kidneys. The detailed mechanism of the saturation behavior in the liver and the pathways involved is still under investigation.

The PET distribution patterns for ^{64}Cu-labeled polymers dPGS-SCN DMPTACN **10** and dPGS-mal DMPTACN **11** are in accordance with the autoradiographic data for the tritium-labeled dPGS **3b**, which indicates that functionalization of the polymer with the chelator does not show any remarkable effect, at least in this case where the extent of modification was kept to a minimum. The similar behavior of **3b** and compounds **10**, **11** also indicates a negligible effect of free amines on the overall in vivo behavior of the polymer.

It is worth noting that processes like aggregation of the polymer and the formation of a protein corona,[39,40] which leads to recognition and elimination by the RES,[32] are likely to be dependent on local concentrations and hence the distribution

DOI: 10.1021/acs.bioconjchem.5b00127
Bioconjugate Chem. 2015, 26, 906−918

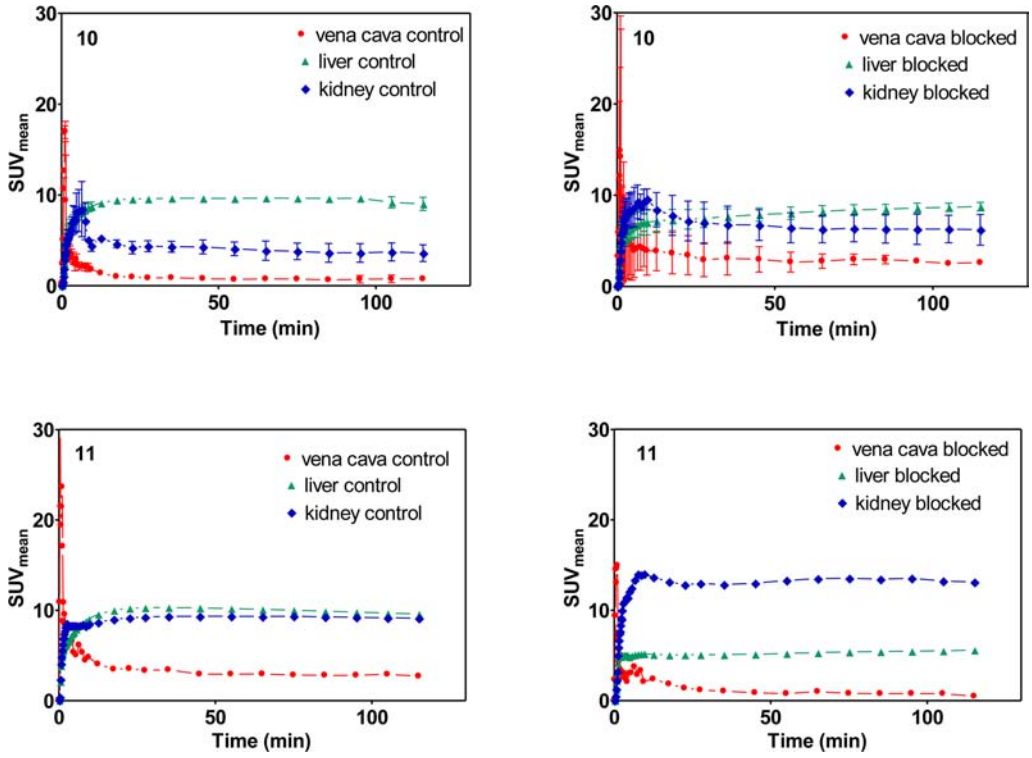

Figure 7. Time−activity concentration curves for ^{64}Cu-labeled dPGS **10** (upper) and **11** (lower) in the blood, liver, and kidneys after single intravenous injection in Wistar rats without (control) or with simultaneous injection of nonradioactive dPGS. Data are given in mean ± SEM (standard error of the mean) and in SUV_{mean}.

profile. Studies aimed at understanding these processes and at identifying the most relevant binding partners of dPGS are currently ongoing.

CONCLUSION

We have established two new strategies for radiolabeling polyglycerol systems to provide reliable insight into the biological fate of potential anti-inflammatory drug candidates based on sulfated dendritic polyglycerol (dPGS) scaffolds as well as the neutral dendritic polyglycerol (dPG) as a control. In brief, ^{3}H-labeling of dPGS was achieved via partial oxidative cleavage of the diol units, followed by reduction with [^{3}H]-$NaBH_4$, and then sulfation using a SO_3 pyridine complex. The chemical stability of the ^{3}H-labeled systems is expected to be higher than that of the previously established ^{35}S-labeled systems, which can potentially undergo sulfoester cleavage in vivo. The ease of access to the ^{3}H-labeled polymers compared to the ^{35}S-labeled versions is also a major advantage. Radioactive ^{64}Cu has been incorporated into the dPG scaffolds by conjugating two new Cu(II) chelators based on DMPTACN to partially aminated dPGS. The resulting ^{64}Cu complexes are highly stable and were successfully employed for radioactivity-based μ-PET detection.

Ex vivo (autoradiography) and in vivo (PET) studies carried out using the ^{3}H- and ^{64}Cu-labeled compounds, respectively, indicate that the ^{64}Cu-labeled dPGS/DMPTACN conjugates **10** and **11** and the ^{3}H-labeled dPGS conjugates **4** and **5** accumulate in the liver, kidney, and spleen, and are present in the organs of the RES even after 30 d. This restricts the applicability of the dendritic polyglycerol sulfates for imaging purposes, but they may still potentially be of use for inflammation-specific targeting and/or other therapeutic applications. The radiolabeling approaches described herein are applicable to the development of other polymeric tools based on, for example, alternate polymer scaffolds. As a part of our ongoing research, we plan to examine in detail the pharmacokinetic behavior of a wide variety of dendritic polymers in order to establish structure−biocompatibility relationships that will guide the development of clinically useful theranostics and multimodal diagnostic agents.

EXPERIMENTAL SECTION

Materials and Methods. All materials and chemicals were purchased from Merck or Sigma-Aldrich and were of reagent grade and used as received unless otherwise stated. Tritiated sodium borohydride with an activity of 100 μCi (37 kBq) was commercially available from PerkinElmer (ref: NET023H100MC) and used as received. The production of ^{64}Cu was performed at a PET cyclotron as described in detail elsewhere.[41,42,44] The yields of the nuclear reaction were between 3.6 and 5.2 GBq (EOB), with specific activities of 150−250 GBq/μmol Cu. The synthesis of DMPTACN (**5**) and conversion to the amino (**5b**) and carboxylic (**5f**) derivatives were carried out according to published procedures.[35,26] Dry reactions were performed in flame-dried glassware and under nitrogen atmosphere. Column chromatography was carried out using neutral aluminum oxide (Sigma-Aldrich). Purification via high-performance liquid chromatography (HPLC) was performed on a Zorbax (2.1 mm × 150 mm, 5 μm) C-8 column (Agilent) using an Äkta chromatography system (GE Healthcare, Germany), with detection at 220 and 254 nm. The *Unicorn 5.11* software was used for peak analysis. Size exclusion chromatography (SEC) was performed using superfine Sephadex G-25 (Aldrich, Germany), packed to a depth of 10 cm in a 2.6-cm-i.d. glass column. Analytical characterization of

DOI: 10.1021/acs.bioconjchem.5b00127
Bioconjugate Chem. 2015, 26, 906−918

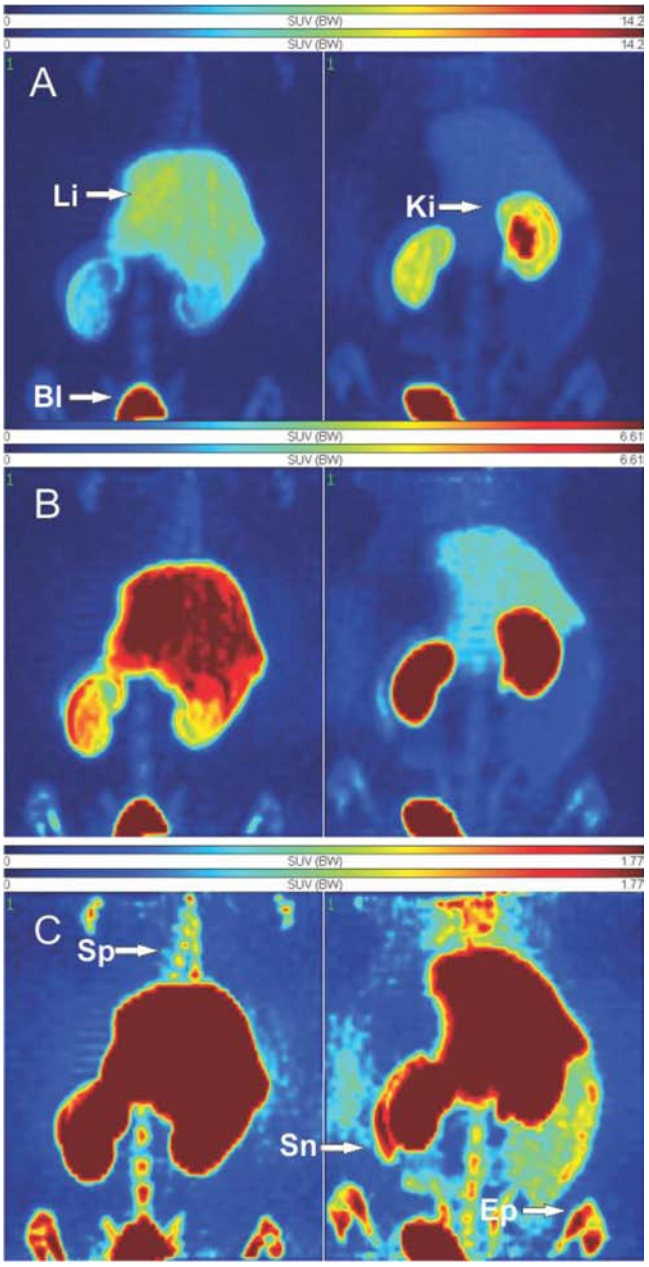

Figure 8. MIPs of two Wistar rats 90 min p.i. after single intravenous injection of 50 μg ^{64}Cu-labeled dPGS **11** in a lateral tail vein, without (left) and with (right) addition of 2.5 mg nonradioactive dPGS in the injection solution (PET/CT). The images were rescaled and are normalized to the identical SUV_{mean} (A), 14.2; (B), 6.61; (C) 1.77, respectively. The signed organs are Li liver, Ki kidneys, Bl bladder, Sp spine, Sn spleen, and Ep epiphysis.

the conjugates was carried out at ambient pressure and 25 °C on a Knauer HPLC system fitted with a UV detector using a PL Aquagel 30 8 μm (7.5 × 300 mm) size exclusion column (Agilent) with Millipore water as an eluent. ^{1}H NMR and ^{13}C NMR spectra were recorded on a 400 MHz Varian Inova spectrometer. Chemical shifts are reported on a δ scale in parts per million (ppm). TMS was used as an internal standard for samples measured in deuterated MeOH. Electrospray ionization mass spectrometry (ESI-MS) was carried out using an expression Compact Mass Spectrometer (Advion). The hydrodynamic size and zeta potential of the polymers were determined at 25 °C via dynamic light scattering (Malvern Zetasizer Nano instrument, USA), with angle detection at 173°. Radio thin layer chromatography (radio-TLC) was performed using instant TLC (iTLC-SG) plates purchased from Agilent Technologies and subsequently read by a radioluminography laser scanner BAS-1800II (Raytest). The *Aida* image analyzer version 4.0 software was used for data analysis. Radio-HPLC and radio-SEC were carried out on a Knauer system fitted with a UV detector and a Gabi radiodetector (Raytest) using Suprema 30 Å 5 μm (300 × 8 mm) column (PSS, Germany) in 0.15 M NaCl as a mobile phase. *ChromeGate* software (v 3.3.2) was used for peak analysis.

Syntheses. *dPG (**1**).* Dendritic polyglycerol with an average number molecular weight (M_n) of 6000 g mol^{-1}, a PDI, (M_w/M_n) of 1.6, and a DB of 60% was prepared according to a literature procedure via a "living" anionic ROMBP reaction using glycidol and a partially deprotonated pentaerythritol starter.[1,30]

*^{3}H-dPG (**2**).* A solution of dPG **1** (500 mg, 83.3 μmol, 6.75 mmol OH groups) in MQ water (2 mL) was cooled to 0 °C and a freshly prepared solution of sodium periodate (144 mg, 68 μmol, 0.1 equiv of OH groups) in MQ water (2 mL) was added over 30 min. The mixture was stirred for 1 h at room temperature (RT) and a solution of sodium sulfite (425 mg, 3.37 mmol) in MQ water (4 mL) was added. The solution was stirred for 1 h at RT and subjected to ultrafiltration (MWCO = 2000 kDa) for 24 h (3 cycles of 30 mL). The volume was reduced to 10 mL and a freshly prepared solution of tritiated sodium borohydride (A = 100 mCi) in a 14 M sodium hydroxide solution (1 mL) was slowly added to the polymer solution at 0 °C. Throughout the Experimental Section the number of significant figures for the millimole value should equal the number given for the mass. The mixture was stirred at RT for 5 h, a solution of inactive sodium borohydride (42.2 mg, 1 mmol) in 14 M sodium hydroxide (1 mL) was added, and the mixture was stirred at RT overnight (O/N). The solution was neutralized by addition of 6 M HCl to a pH value of 8 and the product solution was subjected to ultrafiltration (MWCO = 2000 kDa) for 2 d (9 cycles of 30 mL) until a constant, low radioactivity was detected in the filtrate). The solution was filtered through a 0.45 μm PES filter (VWR, Germany) and the final product was stored in MQ at a concentration of 15 mg mL^{-1} at −196 °C. Specific activity: 192 μCi mg^{-1}, M_n = 6000 g mol^{-1}, yield: 90%, radiochemical yield (RCY) > 80%. Prior to the animal experiments the product was purified by size exclusion chromatography. The analytical data are identical to those of **1**.

*^{3}H-dPGS (DS = 40% (**3a**) and DS = 85% Sulfation (**3b**)).* Dry tritiated dPG **2** (~100 mg) was dried for 2 d at 70 °C and dissolved in anhydrous pyridine (1 mL) and heated to 70 °C. A freshly prepared solution of sulfur trioxide pyridine complex in anhydrous DMF (C = 200 mg mL^{-1}, DS = 40%: 0.55 equiv/OH group; DS = 85%: 1.1 equiv/OH group) was added over a period of 3 h and the solution was stirred for 29 h at 70 °C. The reaction was quenched with MQ water (1 mL) and the pH value was adjusted to 9 by addition of diluted NaOH. The solvent was removed on a vacuum concentrator, the crude product dissolved in MQ, and subjected to ultrafiltration in sodium chloride followed by MQ. **3a**: M_n = 9300 g mol^{-1}, Yield: 75%. S content from combustion analysis: 11.4%, DS = 40%. **3b**: M_n = 13,000 g mol^{-1}, Yield: 81%. S content from combustion analysis: 16.7%, DS = 85%. The spectra of **3a** and **3b** are comparable: ^{1}H NMR (700 MHz, D_2O): δ (ppm) 4.84–

DOI: 10.1021/acs.bioconjchem.5b00127
Bioconjugate Chem. 2015, 26, 906–918

4.60 (C_{sec}H-OSO3Na), 4.49−4.15 ($C_{prim}H_2$−OSO_3Na), 4.14−3.45 (dPG-backbone).

*dPGS Amine (**4**).* Amino-functionalized dPGS (**4**, dPGS amine) was prepared according to the literature, starting from *N*-phthalimide functionalized dPG.[16] In brief, *N*-phthalimide-containing dPG was prepared in a sequential copolymerization of glycidol with *N*-phthalimido glycidol using trimethylol propane (TMP) starter. For dPG amine, the phthalimide groups were cleaved, whereas for dPGS amine (**4**) the deprotection was performed after sulfation. The final product was purified by ultrafiltration and SEC and contained on average 9.5% amino groups corresponding to 4−5 reactive amino groups per polymer. M_n = 10 050 g mol^{-1}, yield: 71%. ^{1}H NMR (700 MHz, D_2O): δ (ppm) 4.89−4.65 (C_{sec}H-OSO_3Na), 4.48−4.17 ($C_{prim}H_2$-OSO_3Na), 4.15−3.30 (m, dPG backbone), 1.53 (s, CH_2CH_3, TMP, 2 H), 1.00 (s, CH_2CH_3, TMP, 3 H) ppm. ^{13}C NMR (176 MHz, D_2O, δ): 78.5, 77.3, 76.1, 75.9, 73.8, 71.1, 70.3, 69.7, 69.5, 68.9, 68.7, 68.3, 67.6, 66.9, 41.2 (C $(CH_2)_4$, TMP), 22.0 (CH_2CH_3, TMP), 7.0 (CH_2CH_3, TMP) ppm. IR (bulk) ν_{max}: 3460, 2952, 2884, 1640, 1460, 1220, 1071, 1027, 1006, 931, 770 cm^{-1}. S content from combustion analysis: 16.6%, DS = 85%.

*2-[4,7-Bis(2-pyridinylmethyl)-1,4,7-triazacyclononan-1-yl]-N-(4-isothiocyanatophenyl)-acetamide (SCN-DMPTACN) (**6**).* Amino DMPTACN (**5b**) (6 mg, 0.013 mmol) was dissolved in a 1:1 (v/v) mixture of dichloromethane and MQ water. To this mixture, a solution of thiophosgene (0.10 mL, 1.3 mol) in dichloromethane (DCM, 1 mL) was slowly added. The solution was stirred for 4 h and the solvent then evaporated using a rotary evaporator. Water (10 mL) was added to the remaining residue and the solution extracted with dichloromethane (2 × 20 mL). The combined aqueous fractions were evaporated under reduced pressure to yield the crude product, which was purified via HPLC system using a 40 min gradient from 100% buffer A (water +0.1%TFA) to 100% buffer B (acetonitrile +0.1%TFA). Yield: 6.4 mg (98%). ^{1}H NMR (400 MHz, D_2O): δ (ppm) 8.67 (d, 2H, pyridyl-CH), 8.47 (m, 2H, pyridyl-CH), 8.05 (d, 2H, aniline-CH), 7.90 (d, 2H, pyridyl-CH), 7.58 (d, 2H, aniline-CH), 7.44 (d, 2H, pyridyl-CH), 4.36 (s, 4H, pyridyl-CH_2), 4.19 (s, 2H, N-CH_2-CO), 3.40 (s, 4H, CH_2-ring), 3.19 (s, 4H, CH_2-ring), 2.95 (s, 4H, CH_2-ring). ^{13}C NMR (101 MHz, CD_3CN): δ 48.1, 49.5, 51.3, 56.8, 57.4, 63.4, 118.2, 121.4, 126.2, 126.8, 127.4, 136.8, 143.4, 145.5, 152.4. ESI-MS: m/z 502.5 $[M + H]^+$, 524.50 $[M + Na]^+$.

*2-[4,7-Bis(2-pyridylmethyl)-1,4,7-triazacyclononan-1-yl]-N-(4-(2-aminoethylmaleimide))-acetamide (mal-DMPTACN) (**7**).* Under an inert atmosphere, a solution of HBTU (12 mg, 0.03 mmol) in anhydrous *N,N*-dimethylformamide (DMF) was added to a solution of DMPTACN-COOH (**5f**) (7.4 mg, 0.02 mmol), followed by diisopropylethylamine (DIPEA) (35 μL, 0.2 mmol). After stirring the solution for 30 min at RT, *N*-(2-aminoethyl) maleimide trifluoroacetate salt (7.62 mg, 0.02 mmol) and DIPEA (6 μL, 0.03 mmol) was added. The mixture was then stirred at RT O/N. The conversion of **5f** to **7** was monitored using ESI-MS. The product was used without further purification because of hydrolytic instability of the maleimide. Yield: 9.1 mg (92%). ESI-MS: m/z 492.42 $[M + H]^+$, 514.39 $[M + Na]^+$.

*dPGS-DMPTACN (**8**) via SCN-DMPTACN (**6**).* dPGS amine (**4**) (20 mg, 2.0 μmol) and **8** (7 mg, 14 μmol) were dissolved in 0.1 M carbonate buffer (pH 9) (300 μL) and the solution stirred for 24 h at RT. The crude product was then purified using SEC. Yield: 85%. The conjugation was confirmed by a sharp band in the SEC column and RP-TLC. The chelator-to-conjugate ratio was found to be 0.96 as determined by radiometric titration (Figure 2A). The conjugates were purified prior to each animal experiment to avoid any aggregation effect on the distribution profile.

*dPGS-DMPTACN (**9**) via mal-DMPTACN (**7**).* Under inert atmosphere, iminothiolane (2.75 mg, 12.7 μmol,) and DIPEA (3.5 μL, 10 μmol) was added to a solution of **4** (20 mg, 1.8 μmol) in anhydrous DMF and water (9:1 v/v). After stirring for 30 min, **7** (6.83 mg, 12.3 μmol) was added and stirring continued for a further 48 h. The product was purified by SEC. Yield: 86%. Product formation was confirmed by ^{1}H NMR and by the presence of a sharp band in the SEC column and RP-TLC. The chelator-to-conjugate ratio was found to be 1.56 as determined by radiometric titration (Figure 2B). ^{1}H NMR (400 MHz, D_2O): δ (ppm) 8.78−8.52 (d, 2H, pyridyl-CH), 8.50−8.20 (d, 2H, pyridyl-CH), 8.04−7.76 (d, 4H, pyridyl-CH), 6.90−6.84 (s, 2H, =CH_2), 4.72−4.50 (C_{sec}H-OSO_3Na), 4.45−4.27 ($C_{prim}H_2$-OSO_3Na), 4.27−3.22 (m, dPG backbone), 3.15−3.10 (s, CH_2-ring), 3.00−2.90 (s, 6H, CH_2-ring), 1.35 (s, CH_2CH_3, TMP, 2 H).

^{64}Cu(II)-Radiolabeling Kinetics. An aqueous solution of $[^{64}Cu]CuCl_2$ (20 MBq) was added to ca. 0.2 mg (1 mg mL^{-1} stock solution) of **8** or **9** in 100 mM MES buffer at pH 5.5 and the final volume made up to 400 μL. The reaction mixtures were shaken at RT for 5 min, which resulted in RCY > 99.9%. The radiolabeling was monitored using radio-TLC at different time intervals (2, 5, 15, 60 min, and 24 h) using iTLC-SG plates with a 1:1 (v/v) solution of 2 M ammonium acetate and methanol as the mobile phase. Radio-SEC confirmed radio-copper complexation: R_f = ^{64}Cu-**10** and ^{64}Cu-**11** ≈ 0, R_f = $^{64}CuCl_2$ ≈ 1. The SEC traces are provided in the Supporting Information (Figure S5).

Ligand Challenge "Transmetalation" Experiments. A solution containing 10 MBq $[^{64}Cu]CuCl_2$ each was added to ca. 0.2 mg of **8** or **9** (1 mg mL^{-1} stock solution) in 100 μL of 100 mM MES buffer (pH 5.5). After complete radio-complexation (monitored using radio-TLC), 100-fold excess of cyclam (1,4,8,11-tetraazacyclotetradecane) was added and the final volume made up to 500 μL with 100 mM MES buffer. This solution was then stirred for 15 min and radio-TLCs recorded at different time intervals (15 min, 2 and 24 h) to determine the degree of transmetalation. This experiment was also repeated using a 1000 M-fold excess of EDTA as an alternative chelator (Figure S7).

Radiometric Titration. Radiometric titrations were conducted using a mixture of radioactive and nonradioactive copper for the determination of the amount of chelator per conjugate. To a 10 μL aliquot of **8** or **9** (0.2 mM stock solution in 100 mM MES buffer, pH 5.5), increasing amounts of a mixture of $[^{64}Cu]CuCl_2$ and $Cu(NO_3)_2$ with a final concentration of 0.4 mM (stock solution) were added to give different conjugate-to-copper ratios of 1:1, 1:4, 1:10, 1:20, and 1:40. The solutions were stirred for 1 h at RT on a thermomixer at 700 rpm. After complete complexation (confirmed using radio-TLC), an 8-fold excess of EDTA was added to each solution vial to remove any nonspecifically bound Cu(II) ions. The resulting solutions were stirred at 37 °C for 40 min at 700 rpm. The RCY was determined via radio-TLC. The number of chelators per conjugate was calculated using the percentage of Cu(II) ions bound to the conjugate.

Biodistribution Studies with ^{3}H-Labeled Compounds. Biodistribution studies with the tritiated polymers **2**, **3a**, and **3b**

DOI: 10.1021/acs.bioconjchem.5b00127
Bioconjugate Chem. 2015, 26, 906−918

were performed in compliance with the National Animal Welfare Regulations at the CEA in Saclay, France. The experiments were approved by the local ethics committee for animal experimentation. Pathogen free animals, 6-week-old, female Balb/c mice weighing 20 g (Charles River Laboratories, L'Arbresle, France) were individually housed in polycarbonate cages in a conventional animal facility and had access ad libitum to food and drink. At different time points (2, 15, 30 min; 1, 4, and 24 h; 10 and 30 d), the animals were first anesthetized with 2% isoflurane and then injected intravenously (bolus) into the tail vein with the polymers (100 μL, C = 1.4 μg μL^{-1}, specific activity = 4.74×10^6, 4.77×10^6, and 5.55×10^6 Bq mg^{-1} for **2**, **3a**, and **3b**, respectively). Blood samples (whole blood cells included) were collected from the sinus retroorbital after anesthetized with 2% isoflurane and the amount of the radioactive polymers was quantified by scintillation counting: 5 μL of sample was added to 5 mL of Ultima Gold Cocktail from PerkinElmer, and the radioactivity was counted in a liquid scintillation counter (TRI-CARB 2100TR, Packard). Quantification of the radioactivity in the urine was performed in the same manner. At given time points (1 h, 4 h, 24 h, and 10 d for the three polymers and an additional 30 d for **2** and **3a**), mice were sacrificed (n = 3 per time point), blood was removed by exsanguination, and saline perfusion was performed to avoid radioactivity contamination of organs by trace of blood. Then, the organs were collected and immediately frozen at −80 °C by immersion in a mixture of dry ice and isopentane. Tissue sections (20-μm-thick) were cut at 20 °C with a slicing microtome (LEICA Microsystems, France). The microtome was carefully cleaned by water/ethanol solution between treatment of each sample to remove any trace of radioactivity and avoid contamination between different organs. The absence of radioactive contaminants in the rinsing solution was controlled by radioimaging of drop samples. The tissue sections were placed on glass slides and were stored in a freezer for optical study or kept at room temperature for 1 day in the presence of silica gel to ensure complete drying for proper radioimaging analysis. A high-performance digital radioimager (β-imager 2000, Biospace Lab, Paris, France) allowing real-time imaging through direct β-particle counting and absolute radioactivity quantification (detection threshold of 0.001 cpm mm^2 for ^{3}H) was used for quantitative determination of the radioactivity in dried tissue sections. Correct calibration of the apparatus was verified between each sample analysis by counting the radioactivity of a reference sample. For quantification of MWCNTs in organs by radioimaging counting, 50 tissue sections were used for each organ to ensure sufficient sampling. These sections were analyzed by radioimaging to determine the Bq/per tissue section volume, which was converted to total radioactivity per organ on the basis of the total volume of each organ (determined by organ weighing).

Small Animal PET. The local animal research committee at the Landesdirektion Dresden approved the animal facilities and the experiments according to institutional guidelines and the German animal welfare regulations. Wistar rats were purchased from Wistar unilever, HsdCpB : Wu, harlan Winkelmann GmbH, Borchen, Germany. The animals received standard food and tap water ad libitum.

Anesthetized, spontaneously breathing healthy Wistar rats were allowed to stabilize for 10 min after preparation. The animals were positioned on a heated bed to maintain the body temperature at 37 °C. The rats received 10−30 MBq (50 μg) of ^{64}Cu-dPGS 10 (4 animals control, 3 animals blocked) and ^{64}Cu-dPGS 11 (4 animals control, 5 animals blocked) in 0.5 mL E-153 intravenously over 1 min into a lateral tail vein. For the blocking experiments, 2.5 mg of nonradioactive dPGS was simultaneously injected with the radioactive **10** and **11**. At the end of the experiment, the animals were deeply anesthetized and sacrificed by an intravenous injection of potassium chloride. Dynamic PET imaging was performed over 2 to 4 h with a microPET P4 scanner (Siemens Medical solutions, Knoxville) or a NanoScanPET/CT (Mediso, Budapest). The activity of the injection solution was measured in a dose calibrator (Isomed 2000, Dresden, Germany) cross-calibrated to the PET scanners. A 10 min transmission scan was recorded during this time for each subject by using a rotating point source of ^{57}Co (microPET) or a whole body CT (NanoScanPET/CT) was acquired. The transmission scans were used to correct the emission scan for γ-ray attenuation caused by body tissues and supporting structures; it was also used to demarcate the body field for image registration. Data acquisition was performed in 3D list mode and the volume data were acquired by iterative reconstruction algorithms with 0.5 mm voxel size length. The image volume data were converted to Siemens ECAT7 format for further processing and were then analyzed using the ROVER software (ABX GmbH, Radeberg, Germany). Masks for defining three-dimensional regions of interest (ROI) were set and the ROIs' were defined. ROI time activity curves (TAC) were derived for the subsequent data analysis. The ROI data and TAC were further analyzed using *R* (*R* is available as Free Software under the terms of the Free Software Foundation's GNU General Public License in source code form) and especially developed program packages (Jörg van den Hoff, Helmholtz-Zentrum Dresden - Rossendorf, Dresden, Germany). The data were calculated in standard uptake value (SUV, in units of grams per milliliter), defined as the tracer concentration at a certain time point normalized to injected dose per unit body weight. The SUV was used for better comparison within animals of different size and weight and with other species. The graphs were calculated with *GraphPad Prism* v 5.00 for Windows (GraphPad Software, San Diego California USA, www.graphpad.com).

■ ASSOCIATED CONTENT

Supporting Information

^{1}H NMR and ESI MS data of **6**; ^{1}H NMR data of **9**; SEC traces of **4**, **8**, and **9**; radio-SEC traces of **10** and **11**; radio-TLC data showing formation and stability of ^{64}Cu(II) complexes with **4**, **8**, and **9**; autoradiographic images of **2**, **3a**, and **3b**. This material is available free of charge via the Internet at http://pubs.acs.org.

■ AUTHOR INFORMATION

Corresponding Authors

*E-mail: vincent.dive@cea.fr. Phone: +33 1 69083585. Fax: +33 1 69089071.

*E-mail: h.stephan@hzdr.de. Phone: +49 3512603091. Fax: +49 3512603232.

*E-mail: haag@chemie.fu-berlin.de. Phone: +49 30 83852633. Fax: +49 30 8384 52633.

Notes

The authors declare no competing financial interest.

DOI: 10.1021/acs.bioconjchem.5b00127
Bioconjugate Chem. 2015, 26, 906−918

■ ACKNOWLEDGMENTS

We thank Brigitte Große and Karin Landrock for excellent technical assistance. D.G. and R.H. thank the collaborative research center SFB765 by the Deutsche Forschungsgemeinschaft (DFG), and the focus area Nanoscale of the Freie Universität Berlin (www.nanoscale.fu-berlin.de). This study is part of a research initiative "Technologie und Medizin – Multimodale Bildgebung zur Aufklärung des in vivo Verhaltens von polymeren Biomaterialien" of the Helmholtz-Portfoliothema. Financial support by the Helmholtz Virtual Institute NanoTracking (Agreement Number VH-VI-421) is gratefully acknowledged. L.S. is very grateful to the Alexander von Humboldt Foundation for a Senior Research Award, the Helmholtz Association for the award of a Helmholtz International Fellowship, and to the Australian Research Council for funding (Project number: DP130100816) and a Discovery Outstanding Researcher Award. B.G. would like to thank the Australian Research Council for a Future Fellowship (FT130100838).

■ REFERENCES

(1) Frey, H., and Haag, R. (2002) Dendritic polyglycerol: a new versatile biocompatible material. *Rev. Mol. Biotechnol. 90*, 257–267.

(2) Calderón, M., Quadir, M. A., Sharma, S. K., and Haag, R. (2010) Dendritic polyglycerols for biomedical applications. *Adv. Mater. 22*, 190–218.

(3) Paez, J. I., Brunetti, V., Strumia, M. C., Becherer, T., Solomun, T., Miguel, J., Hermanns, C. F., Calderón, M., and Haag, R. (2012) Dendritic polyglycerolamine as a functional antifouling coating of gold surfaces. *J. Mater. Chem. 22*, 19488–19497.

(4) Dernedde, J., Rausch, A., Weinhart, M., Enders, S., Tauber, R., Licha, K., Schirner, M., Zügel, U., von Bonin, A., and Haag, R. (2010) Dendritic polyglycerol sulfates as multivalent inhibitors of inflammation. *Proc. Natl. Acad. Sci. U.S.A. 107*, 19679–19684.

(5) Fischer, W., Calderón, M., Schulz, A., Andreou, I., Weber, M., and Haag, R. (2010) Dendritic polyglycerols with oligoamine shells show low toxicity and high siRNA transfection efficiency in vitro. *Bioconjugate Chem. 21*, 1744–1752.

(6) Türk, H., Haag, R., and Alban, S. (2004) Dendritic polyglycerol sulfates as new heparin analogues and potent inhibitors of the complement system. *Bioconjugate Chem. 15*, 162–167.

(7) Licha, K., Welker, P., Weinhart, M., Wegner, N., Kern, S., Reichert, S., Gemeinhardt, I., Weissbach, C., Ebert, B., Haag, R., et al. (2011) Fluorescence imaging with multifunctional polyglycerol sulfates: novel polymeric near-IR probes targeting inflammation. *Bioconjugate Chem. 22*, 2453–2460.

(8) Biffi, S., Dal Monego, S., Dullin, C., Garrovo, C., Bosnjak, B., Licha, K., Welker, P., Epstein, M. M., and Alves, F. (2013) Dendritic polyglycerolsulfate near infrared fluorescent (NIRF) dye conjugate for non-invasively monitoring of inflammation in an allergic asthma mouse model. *PLoS One 8*, e57150.

(9) Kainthan, R. K., and Brooks, D. E. (2007) In vivo biological evaluation of high molecular weight hyperbranched polyglycerols. *Biomaterials 28*, 4779–4787.

(10) Calderón, M., Reichert, S., Welker, P., Licha, K., Kratz, F., and Haag, R. (2014) Receptor mediated cellular uptake of low molecular weight dendritic polyglycerols. *J. Biomed. Nanotechnol. 10*, 92–99.

(11) Garcia, K. P., Zarschler, K., Barbaro, L., Barreto, J. A., O'Malley, W., Spiccia, L., Stephan, H., and Graham, B. (2014) Zwitterionic-coated "stealth" nanoparticles for biomedical applications: recent advances in countering biomolecular corona formation and uptake by the mononuclear phagocyte system. *Small 10*, 2516–2529.

(12) Nel, A. E., Madler, L., Velegol, D., Xia, T., Hoek, E. M. V., Somasundaran, P., Klaessig, F., Castranova, V., and Thompson, M. (2009) Understanding biophysicochemical interactions at the nano-bio interface. *Nat. Mater. 8*, 543–557.

(13) Akesson, A., Cardenas, M., Elia, G., Monopoli, M. P., and Dawson, K. A. (2012) The protein corona of dendrimers: PAMAM binds and activates complement proteins in human plasma in a generation dependent manner. *RSC Adv. 2*, 11245–11248.

(14) Walkey, C. D., and Chan, W. C. (2012) Understanding and controlling the interaction of nanomaterials with proteins in a physiological environment. *Chem. Soc. Rev. 41*, 2780–2799.

(15) Balogh, L., Nigavekar, S. S., Nair, B. M., Lesniak, W., Zhang, C., Sung, L. Y., Kariapper, M. S. T., El-Jawahri, A., Llanes, M., Bolton, B., et al. (2007) Significant effect of size on the in vivo biodistribution of gold composite nanodevices in mouse tumor models. *Nanomed. Nanotechnol. Biol. Med. 3*, 281–296.

(16) Gröger, D., Paulus, F., Licha, K., Welker, P., Weinhart, M., Holzhausen, C., Mundhenk, L., Gruber, A. D., Abram, U., and Haag, R. (2013) Synthesis and biological evaluation of radio and dye labeled amino functionalized dendritic polyglycerol sulfates as multivalent anti-inflammatory compounds. *Bioconjugate Chem. 24*, 1507–1514.

(17) Holzhausen, C., Gröger, D., Mundhenk, L., Welker, P., Haag, R., and Gruber, A. D. (2013) Tissue and cellular localization of nanoparticles using 35S labeling and light microscopic autoradiography. *Nanomed. Nanotechnol. Biol. Med. 9*, 465–468.

(18) Wu, C., Li, F., Niu, G., and Chen, X. (2013) PET imaging of inflammation biomarkers. *Theranostics 3*, 448–66.

(19) Shokeen, M., and Anderson, C. J. (2009) Molecular imaging of cancer with copper-64 radiopharmaceuticals and positron emission tomography (PET). *Acc. Chem. Res. 42*, 832–841.

(20) Smith, S. V. (2004) Molecular imaging with copper-64. *J. Inorg. Biochem. 98*, 1874–901.

(21) Blower, P. J., Lewis, J. S., and Zweit, J. (1996) Copper radionuclides and radiopharmaceuticals in nuclear medicine. *Nucl. Med. Biol. 23*, 957–980.

(22) Bartholoma, M. D. (2012) Recent developments in the design of bifunctional chelators for metal-based radiopharmaceuticals used in Positron Emission Tomography. *Inorg. Chim. Acta 389*, 36–51.

(23) Delgado, R., Felix, V., Lima, L. M. P., and Price, D. W. (2007) Metal complexes of cyclen and cyclam derivatives useful for medical applications: a discussion based on thermodynamic stability constants and structural data. *Dalton Trans. 26*, 2734–2745.

(24) Juran, S., Walther, M., Stephan, H., Bergmann, R., Steinbach, J., Kraus, W., Emmerling, F., and Comba, P. (2009) Hexadentate bispidine derivatives as versatile bifunctional chelate agents for copper(II) radioisotopes. *Bioconjugate Chem. 20*, 347–359.

(25) Comba, P., Hunoldt, S., Morgen, M., Pietzsch, J., Stephan, H., and Wadepohl, H. (2013) Optimization of pentadentate bispidines as bifunctional chelators for Cu-64 positron emission tomography (PET). *Inorg. Chem. 52*, 8131–8143.

(26) Gasser, G., Tjioe, L., Graham, B., Belousoff, M. J., Juran, S., Walther, M., Künstler, J. U., Bergmann, R., Stephan, H., and Spiccia, L. (2008) Synthesis, copper(II) complexation, ^{64}Cu-labeling, and bioconjugation of a new bis(2-pyridylmethyl) derivative of 1,4,7-triazacyclononane. *Bioconjugate Chem. 19*, 719–30.

(27) Barreto, J. A., Matterna, M., Graham, B., Stephan, H., and Spiccia, L. (2011) Synthesis, colloidal stability and Cu-64 labeling of iron oxide nanoparticles bearing different macrocyclic ligands. *New J. Chem. 35*, 2705–2712.

(28) Bergmann, R., Ruffani, A., Graham, B., Spiccia, L., Steinbach, J., Pietzsch, J., and Stephan, H. (2013) Synthesis and radiopharmacological evaluation of ^{64}Cu-labeled bombesin analogs featuring a bis(2-pyridylmethyl)-1,4,7 triazacyclononane chelator. *Eur. J. Med. Chem. 70*, 434–446.

(29) Viehweger, K., Barbaro, L., Garcia, K. P., Joshi, T., Geipel, G., Steinbach, J., Stephan, H., Spiccia, L., and Graham, B. (2014) EGF receptor-targeting peptide conjugate incorporating a near-IR fluorescent dye and a novel 1,4,7-triazacyclononane-based ^{64}Cu(II) chelator assembled via click chemistry. *Bioconjugate Chem. 25*, 1011–22.

(30) Sunder, A., Hanselmann, R., Frey, H., and Mulhaupt, R. (1999) Controlled synthesis of hyperbranched polyglycerols by ring-opening multibranching polymerization. *Macromolecules 32*, 4240–4246.

DOI: 10.1021/acs.bioconjchem.5b00127
Bioconjugate Chem. 2015, 26, 906–918

(31) Fukuda, M. (2001) Chemical Labeling of Carbohydrates by Oxidation and Sodium Borohydride Reduction. In *Current Protocols in Molecular Biology*, John Wiley & Sons, Inc.
(32) Chapanian, R., Constantinescu, I., Brooks, D. E., Scott, M. D., and Kizhakkedathu, J. N. (2012) In vivo circulation, clearance, and biodistribution of polyglycerol grafted functional red blood cells. *Biomaterials 33*, 3047−3057.
(33) Imran ul-Haq, M., Lai, B. F., and Kizhakkedathu, J. N. (2014) Hybrid polyglycerols with long blood circulation synthesis, biocompatibility, and biodistribution. *Macromol. Biosci. 14*, 1469−1482.
(34) Weinhart, M., Gröger, D., Enders, S., Riese, S. B., Dernedde, J., Kainthan, R. K., Brooks, D. E., and Haag, R. (2011) The role of dimension in multivalent binding events: structure−activity relationship of dendritic polyglycerol sulfate binding to L-selectin in correlation with size and surface charge density. *Macromol. Biosci. 11*, 1088−1098.
(35) Pombo-Garcia, K., Zarschler, K., Barreto, J. A., Hesse, J., Spiccia, L., Graham, B., and Stephan, H. (2013) Design, synthesis, characterisation and in vitro studies of hydrophilic, colloidally stable, ^{64}Cu- (II)-labelled, ultrasmall iron oxide nanoparticles in a range of human cell lines. *RSC Adv. 3*, 22443−22454.
(36) Meares, C. F., McCall, M. J., Reardan, D. T., Goodwin, D. A., Diamanti, C. I., and Mctigue, M. (1984) Conjugation of antibodies with bifunctional chelating-agents - isothiocyanate and bromoacetamide reagents, methods of analysis, and subsequent addition of metal-ions. *Anal. Biochem. 142*, 68−78.
(37) Langford, J. H., Cooper, M. S., and Orchard, K. H. (2011) Development and validation of the ^{57}Co assay for determining the ligand to antibody ratio in bifunctional chelate/antibody conjugates for use in radioimmunotherapy. *Nucl.Med. Biol. 38*, 1103−10.
(38) Gröger, D., Kerschnitzki, M., Weinhart, M., Reimann, S., Schneider, T., Kohl, B., Wagermaier, W., Schulze-Tanzil, G., Fratzl, P., and Haag, R. (2014) Selectivity in bone targeting with multivalent dendritic polyanion dye conjugates. *Adv. Healthcare Mater. 3*, 375−85.
(39) Zarschler, K., Prapainop, K., Mahon, E., Rocks, L., Bramini, M., Kelly, P. M., Stephan, H., and Dawson, K. A. (2014) Diagnostic nanoparticle targeting of the EGF-receptor in complex biological conditions using single-domain antibodies. *Nanoscale 6*, 6046−56.
(40) Lynch, I., Salvati, A., and Dawson, K. A. (2009) Protein-nanoparticle interactions what does the cell see? *Nat. Nanotechnol. 4*, 546−547.
(41) Szelecsenyi, F., Blessing, G., and Qaim, S. M. (1993) Excitation-functions of proton-induced nuclear-reactions on enriched Ni-61 and Ni-64 - possibility of production of no-carrier-added Cu-61 and Cu-64 at a small cyclotron. *Appl. Radiat. Isot. 44*, 575−580.
(42) McCarthy, D. W., Shefer, R. E., Klinkowstein, R. E., Bass, L. A., Margeneau, W. H., Cutler, C. S., Anderson, C. J., and Welch, M. J. (1997) Efficient production of high specific activity Cu-64 using a biomedical cyclotron. *Nucl. Med. Biol. 24*, 35−43.
(43) Erhardt, J. M., Grover, E. R., and Wuest, J. D. (1980) Transfer of hydrogen from orthoamides - synthesis, structure, and reactions of hexahydro-6bh-2a,4a,6a-triazacyclopenta[Cd]-pentalene and perhydro-3a,6a,9a-triazaphenalene. *J. Am. Chem. Soc. 102*, 6365−6369.
(44) Thieme, S., Walther, M., Preusche, S., Rajander, J., Pietzsch, H.-J., Lill, J. O., Kaden, M., Solin, O., and Steinbach, J. (2013) High specific activity ^{61}Cu via ^{64}Zn (p,a) ^{61}Cu reaction at low proton energies. *Appl. Radiat. Isot. 72*, 169−76.
(45) Kimberly, A. L., Ferdani, R., Liang, K., Zheleznyak, A., Andrews, R., Sherman, C., Achilefu, S., Anderson, C., and Rogers, B. (2011) In vitro and in vivo evaluation of ^{64}Cu-labeled SarAr-bombesin analogs in gastrin-releasing peptide receptor−expressing prostate cancer. *J. Nucl. Med. 52*, 470−477.
(46) Lundqvist, M., Stigler, J., Elia, G., Lynch, I., Cedervall, T., and Dawson, K. A. (2008) Nanoparticle size and surface properties determine the protein corona with possible implications for biological impacts. *Proc. Natl. Acad. Sci. U.S.A. 105*, 14265−14270.
(47) Czarny, B., Georgin, D., Berthon, F., Plastow, G., Pinault, M., Patriarche, G., L'Thuleau, A., Hermite, M., Taran, F., and Dive, V. (2014) Carbon nanotube translocation to distant organs after pulmonary exposure: Insights from in situ 14C- radiolabeling and tissue radioimaging. *ACS Nano 8*, 5715−5724.
(48) Melis, M., de Swart, J., de Visser, M., Berndsen, S. C., Koelewijn, S., Velkema, R., Boerman, O. C., Krennin, E. P., and de Jong, M. (2010) Dynamic and static small-snimal SPECT in rats for monitoring renal function after ^{177}Lu-labeled Tyr3-octreotate radionuclide therapy. *J. Nucl. Med. 51*, 1962−1968.

DOI: 10.1021/acs.bioconjchem.5b00127
Bioconjugate Chem. 2015, 26, 906−918